Journal of
Medicinal Chemistry

Article

Pre-clinical lead optimization of a 1,2,4-triazole based tankyrase inhibitor

Jo Waaler, Ruben Leenders, Sven T. Sowa, Shoshy Alam Brinch, Max Lycke, Piotr Nieczypor, Sjoerd Aertssen, Sudarshan Murthy, Albert Galera-Prat, Eddy Damen, Anita Wegert, Marc Nazare, Lari Lehtiö, and Stefan Krauss

J. Med. Chem., **Just Accepted Manuscript** • DOI: 10.1021/acs.jmedchem.0c00208 • Publication Date (Web): 08 Jun 2020

Just Accepted

is published by the American Chemical Society. 1155 Sixteenth Street N.W., Washington, DC 20036

Pre-clinical lead optimization of a 1,2,4-triazole based tankyrase inhibitor

Jo Waaler,[*,†,‡,#] Ruben G. G. Leenders,[§,#] Sven T. Sowa,[|,#] Shoshy Alam Brinch,[†,‡] Max Lycke,[†,‡] Piotr Nieczypor,[§] Sjoerd Aertssen,[§] Sudarshan Murthy,[|] Albert Galera-Prat,[|] Eddy Damen,[§] Anita Wegert,[§] Marc Nazaré,[||] Lari Lehtiö,[|] and Stefan Krauss[†,‡]

[†]Hybrid Technology Hub - Centre of Excellence, Institute of Basic Medical Sciences, University of Oslo, P.O. Box 1110 Blindern, 0317, Oslo, Norway.
[‡]Department of Immunology and Transfusion Medicine, Oslo University Hospital, P.O. Box 4950 Nydalen, 0424, Oslo, Norway.
[§]Mercachem BV, Kerkenbos 1013, 6546 BB Nijmegen, the Netherlands.
[|]Faculty of Biochemistry and Molecular Medicine, Biocenter Oulu, University of Oulu, PO Box 5400, 90014 Oulu, Finland.
[||]Medicinal Chemistry, Leibniz-Forschungsinstitut für Molekulare Pharmakologie (FMP), Campus Berlin Buch, Robert-Roessle-Str. 10, 13125, Berlin, Germany.

KEYWORDS Tankyrase, WNT/β-catenin signaling, Hippo signaling, cell signaling, cancer treatment

ABSTRACT: Tankyrases 1 and 2 are central biotargets in the WNT/β-catenin signaling and Hippo signaling pathways. We have previously developed tankyrase inhibitors bearing a 1,2,4-triazole moiety and binding predominantly to the adenosine binding site of the tankyrase catalytic domain. Here we describe a systematic structure-guided lead optimization approach of these tankyrase inhibitors. The central 1,2,4-triazole template and *trans*-cyclobutyl linker of the lead compound **1** were left unchanged, while side-group East-, West- and South-moieties were altered by introducing different building blocks defined as point mutations. The systematic study provided a novel series of compounds reaching picomolar IC_{50} inhibition in WNT/β-catenin signaling cellular reporter assay. The novel optimized lead **13** resolves previous atropisomerism, solubility and Caco-2 efflux liabilities. **13** shows a favorable ADME profile, including improved Caco-2 permeability and oral bioavailability in mice, and exhibits anti-proliferative efficacy in the colon cancer cell line COLO 320DM *in vitro*.

INTRODUCTION Tankyrase 1 and tankyrase 2 (TNKS1/2) are members of the PARP family of enzymes that control protein activities, interactions and turn-over through mono- or poly-ADP-ribosylation.[1] TNKS1/2 regulate a number of target proteins, including AXIN1 and AXIN2 (AXIN1/2) in the β-catenin destruction complex resulting in WNT/β-catenin signaling pathway inhibition, and AMOT proteins in the Hippo signaling pathway resulting in YAP signaling inhibition.[1-3] Tankyrases, through their ankyrin repeat clusters, bind to AXIN1/2, making AXIN1/2 accessible for ADP-ribosylation by the C-terminal TNKS1/2 catalytic domain.[1] AXIN1/2 is subsequently targeted for proteasomal degradation through poly-ubiquitination of E3 ubiquitin ligase RNF146, recognizing the poly-ADP-ribose signal.[1, 2] Destabilization of AXIN1/2, being a structural protein in the β-catenin destruction complex, leads to increased β-catenin levels which can be counteracted by inhibition of TNKS1/2 catalytic activity.[1, 2] Similarly, TNKS1/2 control the stability of AMOT proteins via RNF146. Stabilization of AMOT proteins by inhibiting TNKS1/2 activity sequesters YAP to the cytoplasm and prevents target gene expression driven by YAP in the nucleus.[1, 3] TNKS1/2 catalytic activities also interfere with other biological mechanisms and cell signaling pathways such as vesicle transport, energy metabolism, telomere homeostasis and mitotic spindle formation as well as

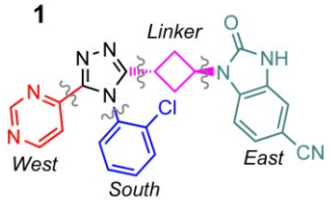

Figure 1. Lead compound **1** and the building blocks defined as West (red), South (blue), East (green) and linker (pink).

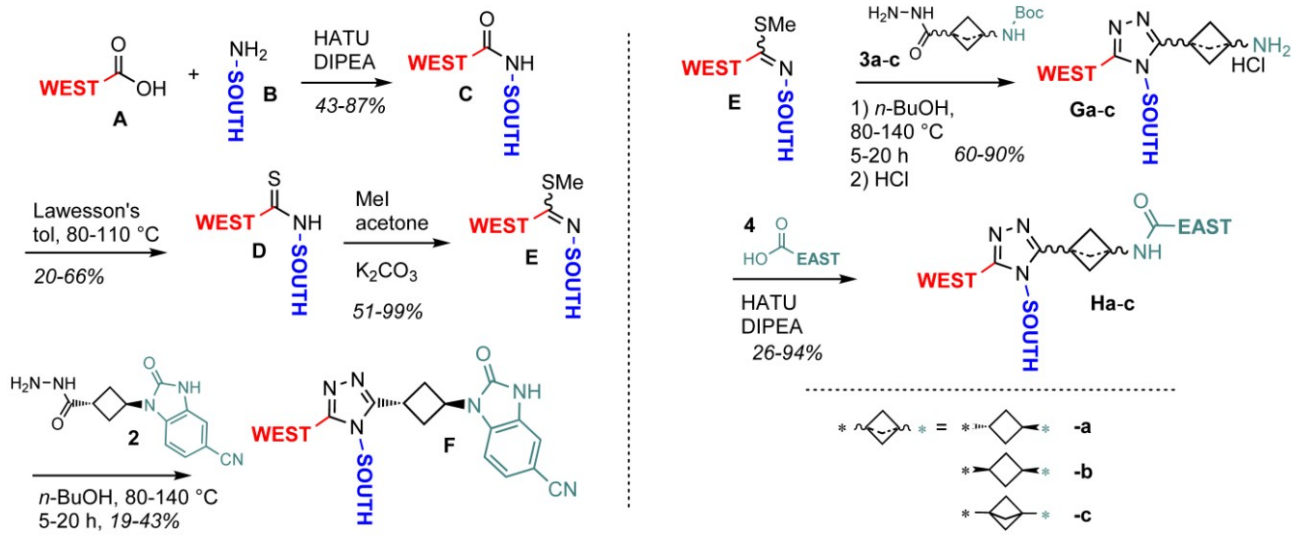

Scheme 1. (a) Synthesis of targets with South and West variations. (b) Synthesis of targets with East variations.

affecting components in AKT/PI3K and AMPK signaling pathways.[1, 4-6]

Several groups of chemical substances have been identified which inhibit TNKS1/2 by binding to the substrate NAD^+ binding site either by occupying a nicotinamide pocket, adenosine binding pocket, or by addressing both of them.[2, 7-20] Although the catalytic domains of 17 human ARTD/PARP enzymes are homologous, unique features in the TNKS1/2 catalytic domain allow the development of tankyrase-selective chemical inhibitors.[1] Despite this progress, there is currently no viable selective TNKS1/2 inhibitor in clinical testing or practice for any application including targeting the WNT/β-catenin and YAP signaling pathways in cancer therapy.[17, 21-23]

It has been shown that TNKS1/2 inhibitors can exhibit anti-cancer efficacy in mouse models, either as monotherapy against colorectal cancer[8, 24] and osteosarcoma[25], or in combination therapies together with PI3K and EGFR inhibitors against colorectal cancer[26] or with PD-1 inhibition against melanoma.[27]

Two reports indicate intestinal toxicity[24] and bone loss[28] in mouse models upon treatment with early lead-stage tankyrase inhibitors while other reports do not document signs of toxicity, intestinal injury or body weight changes.[8, 26, 27, 29] Hence, there is a continued need for the development of safe drugs directed towards TNKS1/2 and the WNT/β-catenin signaling pathway with improved chemical and biophysical properties.[17, 21-23]

The compound optimization described here is based on the understanding of the structure activity relationship, crystallography and physicochemical properties of our previous 1,2,4-triazole analogue series JW74,[30] G007-LK[9] and OD336 (**1**)(compound 16[11]). The optimization focused especially on the solubility and atropisomerism liabilities of the former G007-LK and **1** compounds, respectively. In our work we developed a novel series of compounds reaching picomolar IC_{50} activity in a cellular WNT/β-catenin signaling reporter assay. Lead compound OM-1700 (**13**), within the novel series displays high potency and specificity, and has overall favorable ADME properties compared to benchmark tankyrase inhibitors.

RESULTS AND DISCUSSION

Chemistry. For the synthesis of novel structures in the optimization campaign, we embraced a building block approach (Figure 1). Herein we were able to prepare all compounds following the same synthetic route, simplifying synthesis efforts (Scheme 1). Cyclic amide/urea/carbamate East-modifications however, re-

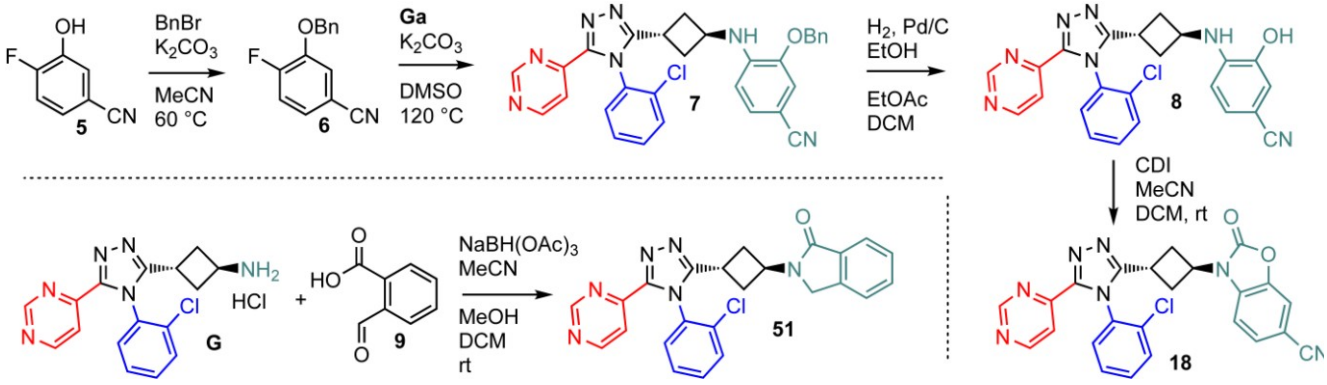

Scheme 2. Synthesis of **18** and **51**

a)

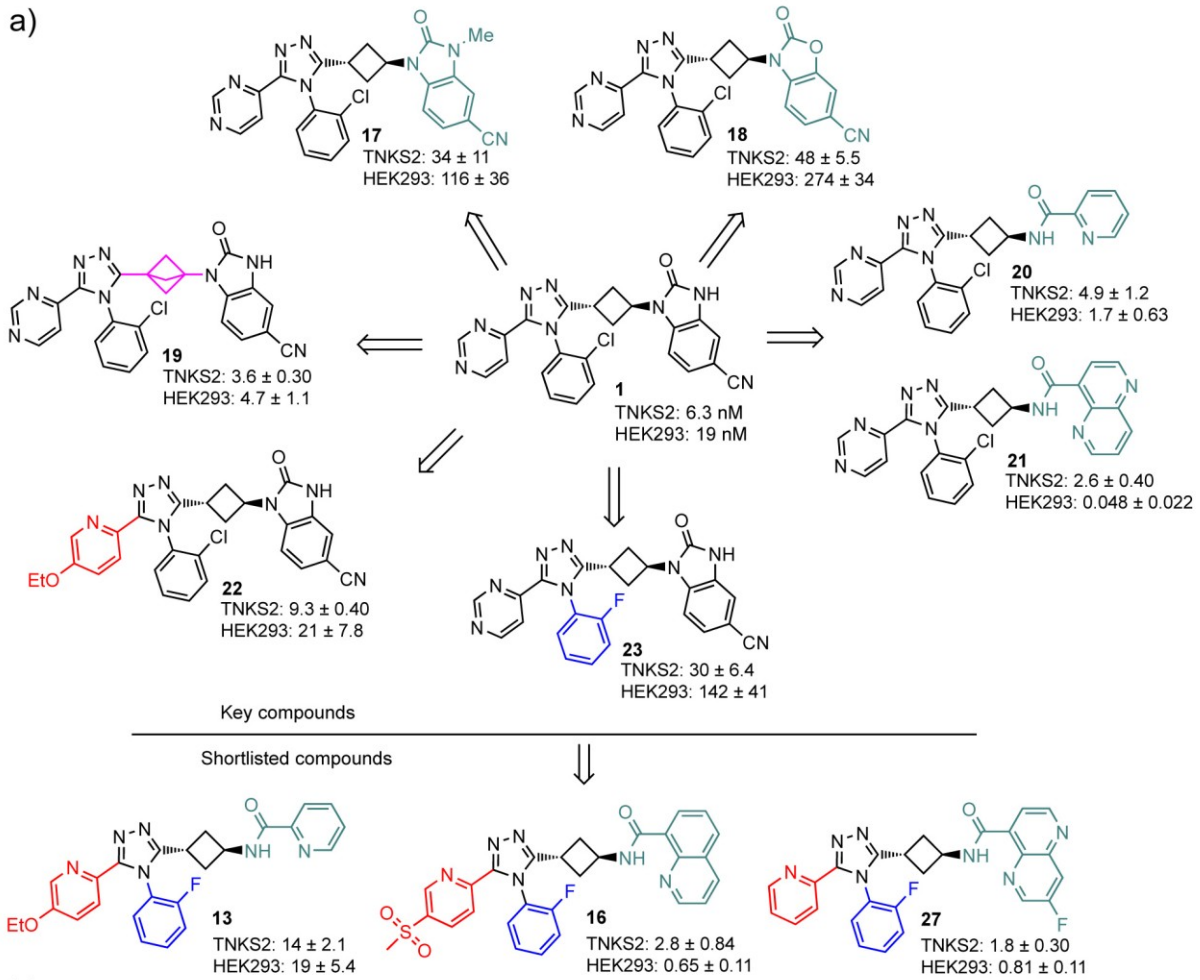

b)

ID	Kinetic Solubility pH 7.4 (μM)	Caco-2 permeability P_{app} AB (10^{-6} cm/s) / efflux ratio	Microsomal stability CL_{int} (μL/min/mg protein) / $t_{1/2}$ (min)	
			human	mouse
1	12	10 / 4.2	242 / 6	204 / 7
19	1.5	5.0 / 5.3	200 / 7	256 / 5
20	>80		<15 / >90	125 / 11
21	79	31 / 1.2	227 / 6	411 / 3
22			<15 / >90	57 / 24

c)

ID	HEK293 IC50 (nM ± SD)	$T_{1/2}$ (h)	T_{max} (h)	C_{max} (ng/mL)	AUC 0→t (ng/mL*h)	AUC 0→∞ (ng/mL*h)	MRT 0→∞ (h)	Vd (L/Kg)	CL (L/h/Kg)
1	19	1.51	0.25	124	145	147	1.61	74.2	34.0
13	19 ± 5.4	0.67	0.25	3203	2384	2388	0.69	2.03	2.09
16	0.65 ± 0.11	0.76	0.5	1448	2955	2963	1.73	1.86	1.69
27	0.81 ± 0.11	0.95	0.25	3419	5033	5057	1.43	1.35	0.99

Figure 2. (a) Selected key compounds in the optimization campaign and respective TNKS2 and HEK293 IC_{50} values. Means ± SD for three independent experiments are shown. Moieties in color when differing from **1**. (b) ADME data of key compounds. (c) Cellular efficacy and mouse PO PK 5 mg/kg of the shortlisted compounds.

quired a different route (Scheme 2). Since the 1,2,4-triazole as a central scaffold was well established in our previous research,[9] it was left unchanged in the present lead optimization process. In the linker area between the 1,2,4-triazole and the East-moieties, we synthesized a series of analogues with a bicyclo[1.1.1]pentane configuration and one compound with a *cis*-cyclobutane setup. These linker variations were synthesized according to the same scheme as for the default *trans* linker. For further optimization, the *trans*-cyclobutyl linker was left unchanged for the majority of the target molecules as it proved to be superior to the tested alternative linker iterations.[11]

For compounds having the benzimidazolone West-moiety of **1**, synthesis was performed as depicted in Scheme 1a and described in our previous work.[11] For East-side variations, a slightly different route enabling East variations in the last step departing from amine **G** was used (Scheme 1b).

As a first iteration, we replaced the East benzimidazolone group as in our experience this group can result in unwanted solubility, permeability and efflux properties. When suitable East-amides were identified as a replacement for the benzimidazolone group, a wide range of further options for East-side iterations opened enabling fine-tuning of physico-chemical properties. Next we replaced the West-pyrimidine as this group renders the molecule vulnerable for CYP-mediated oxidation which was confirmed by Med-Id studies of **1**.

To synthesize a broad set of targets, we optimized the triazole-forming reaction from **E** to **G** (Scheme 1b) from the existing method (TFA, DMA, 120 °C, 14h, 10-21% yield). Here, we found that heating of **E** and **3a** in 1-butanol at 80-140 °C for 5 to 20 hours depending on the actual substrate, typically resulted in 60-90% yield. Under these conditions, a broader scope of South- and West-moieties was tolerated in the reaction. All compounds in the present study were prepared accordingly except the benzisoxazolone **18** and lactam **51** (Scheme 2). For compounds with the *cis*-cyclobutane (**75**) and bicyclo[1.1.1]pentane (**19**) moieties, the corresponding hydrazides **3b** and **3c** respectively were used (Scheme 1b).

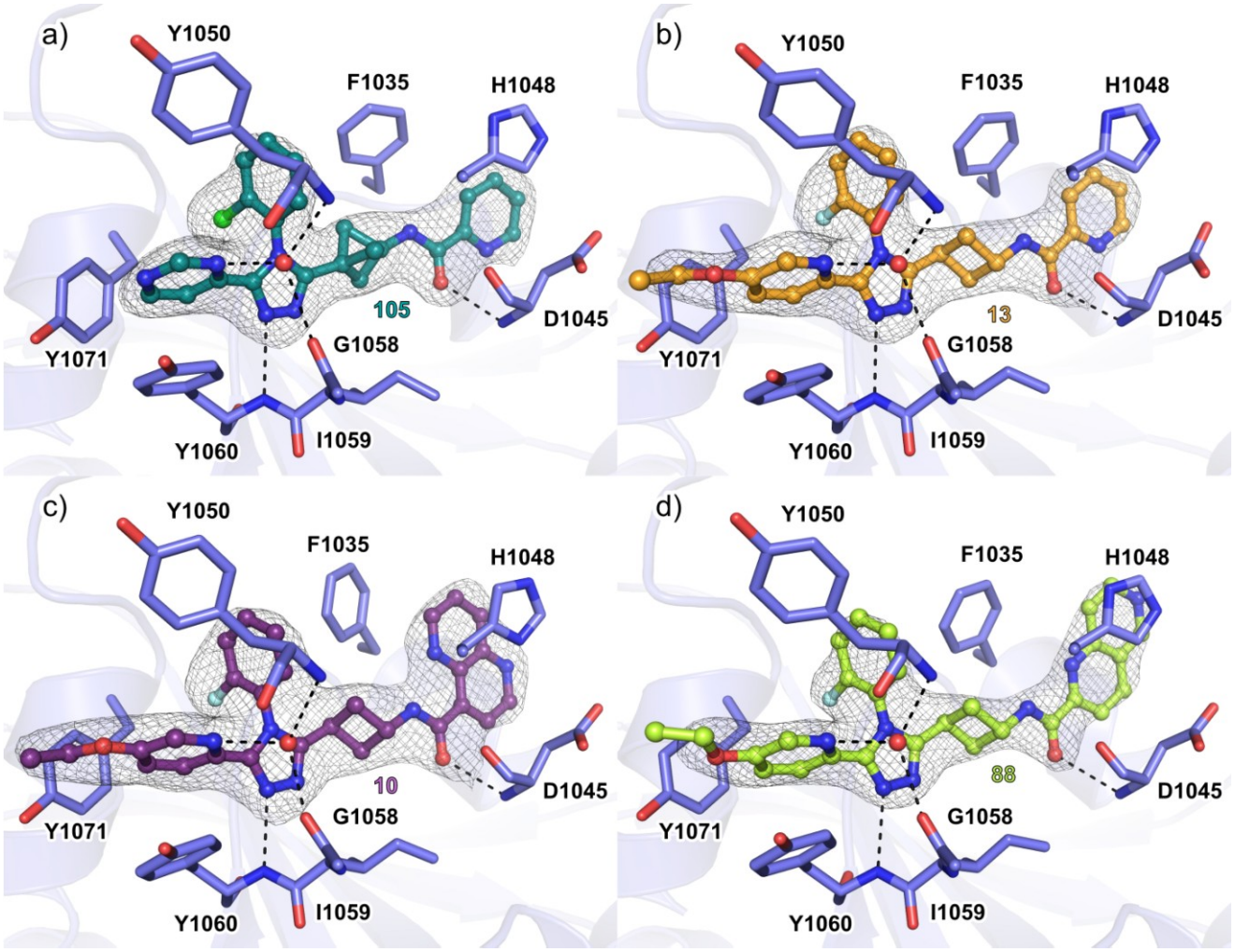

Figure 3. Co-crystal structures of TNKS2 with inhibitors. (a) Binding mode of **105** with TNKS2 catalytic domain (PDB code 6TKN). (b) Binding mode of **13** with TNKS2 catalytic domain (PDB code 6TG4). (c) Binding mode of **10** with TNKS2 catalytic domain (PDB code 6TKM). (d) Binding mode of **88** with TNKS2 catalytic domain (PDB code 6TKS). The dashed lines in black represent hydrogen bonds, and the red spheres represent water molecules. The σ_A weighted $2F_o–F_c$ electron density maps around the ligands are contoured at 1.4-1.7σ. Structures were solved with molecular replacement using the structure of TNKS2 (PDB code 5NOB) as a starting model.

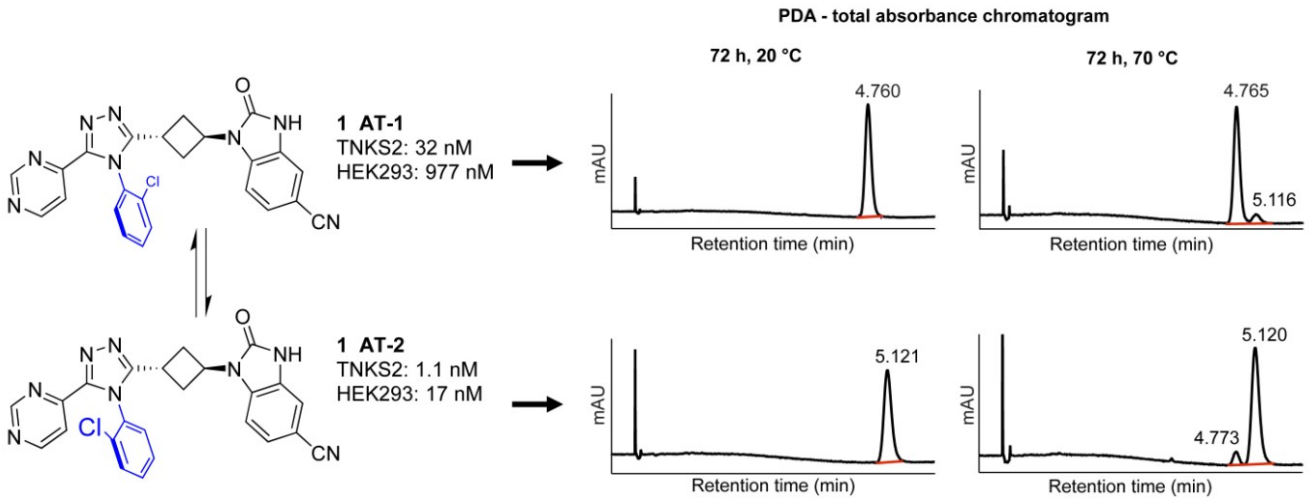

Figure 4. Atropisomerism of **1** (stereochemistry arbitrarily assigned) on chiral SFC and TNKS2 and HEK293 IC_{50} values.

Biological Evaluation. All compounds were tested using a TNKS2 biochemical assay and a luciferase-based WNT/β-catenin signaling pathway reporter assay in human HEK293 cells.[9] In the first round of the optimization campaign, we prepared single-point modifications changing any of the four regions in **1** (Figure 1), while leaving the other regions constant. In the following stages of the optimization campaign, additional East-, West- and South-moieties were also utilized, combining the best structural elements of the first single-point modification round. For the optimization, *in vitro* ADME properties and solubility of selected compounds were measured. Mouse pharmacokinetics, after oral dosing, was tested for the selected and short-listed compounds **13**, **16** and **27** (Figure 2c and indicated by # in Table 1 and 2).

Since **1** displayed low solubility and high Caco-2 efflux,[11] we substituted the benzimidazolone NH-group by forming the *N*-Me variant **17**[31], however, this resulted in a 20-fold less efficacious compound (Figure 2a). Likewise, the oxygen-containing analogue **18** displayed decreased efficacy when compared to **1** (Figure 2a). We then replaced the benzimidazolone moiety,[10, 20] as this can inflict high efflux and low solubility, by a series of East-positioned amides. From these amides, **20** and **21** turned out to be the most potent resulting in picomolar cellular inhibitory IC_{50} efficacies (Figure 2a). Solubility and Caco-2 cell permeation were completely restored in **21** (Figure 2b). The amide having the *N*-Me-group (**44**) was inactive, whereas activity was restored in the cyclic version (**51**) (Supplementary Table 1a). Non-aromatic amides (**52**, **53** and **54**) resulted in inactive compounds (Supplementary Table 1a).

To interrogate the West-side of the pharmacophore, pyridine and pyrimidine analogues were prepared. These compounds inhibited the cellular WNT/β-catenin signaling pathway reporter assay to a similar extent as lead **1**, except the 2-pyrimidyl substituted compound (**56**). The ethoxypyridyl derivative **22** was consequently selected as a starting point for further hybrid synthesis (Figure 2a and Supplementary Table 1b). Introduction of thiazoles to replace the 6-membered heterocycle resulted in less efficacious compounds, with **59** displaying the most favorable properties in this cluster (Supplementary Table 1b). Introduction of aliphatic rings, such as cyclopentane in **63** and cyclopropane in **64**, indicated that aromatic ring systems are required in this position for maintaining potency (Supplementary Table 1b).

Next, in a series of synthesized South-aryl products, the 2-trifluoromethyl (**66**) showed comparable activities to the previous lead **1** (Supplementary Table 1b). The thiophenyl moeity as a bioisosteric replacement for the aryl group was less tolerated while cycloalkyl replacements resulted in activities in the micromolar range (Supplementary Table 1c).

Linker-variations were addressed with the *cis*-cyclobutyl- and bicyclo[1.1.1]pentane-linkers **75** and **19** respectively (Supplementary Table 1d). Compound **75** displayed decreased potency (Supplementary Table 1d) while compound **19** suffered from low solubility (Figure 2b). Despite the more rigid geometry of the bicyclo[1.1.1]pentane in comparison to *trans*-cyclobutyl of **1**, the co-crystal structure with TNKS2 showed a very similar binding mode at the NAD^+ binding cleft (Figure 3). **105** occupied the adenosine sub-pocket and formed the typical hydrogen bonds to the backbone amides of Tyr1060 and Asp1045 (Figure 3a and Supplementary Fig. 1a). A water molecule forms bridging interactions between the pyridine nitrogen and Gly1058 and Tyr1050 and the same applies to all the co-crystal structures described (Figure 3a).

Rotational isomerism (atropisomerism) is a known phenomenon for substituted triazoles and can potentially lead to complexity and challenges for the drug discovery and development processes as atropisomers might have differing biological activities towards a target, different off-target profiles and different pharmacokinetic properties.[32, 33] Since **1** does not contain asymmetric centers, atropisomers are mirror images (enantiomers). Hence, on an achiral HPLC column, as well as in NMR, such atropisomers are indiscernible. In contrast, on a chiral SFC column, lead **1** showed two signals indicating rotational isomerism (Figure 4). When separated, these isomers did not interconvert at 20 °C for 72 hours, but showed a minor interconversion at 70 °C during 72 hours (Figure 4). Interestingly, both isomers, **1**-AT-1 and **1**-AT-2, differed in potency and efficacy with a factor of 30 to almost 60, respectively (Figure 4). To investigate whether atropisomerism was induced by

ID	Hybrids	TNKS2 IC_{50} (nM)	HEK293 IC_{50} (nM)	Kinetic Solubility pH 7.4 (μM)	Caco-2 permeability P_{app} AB (10^{-6} cm/s) / efflux ratio	Microsomal stability CL_{int} (μL/min/mg prot.) / $t_{1/2}$ (min)	
						human	mouse
10	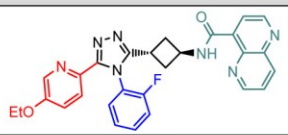	4.3	0.63	>80	34 / 0.6	24 / 58	203 / 8
11	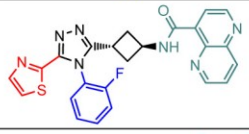	3.3	3.9	2.9	34 / 0.8		
12	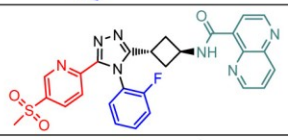	1.1	0.42		3.8 / 18	36 / 39	41 / 33
13 #	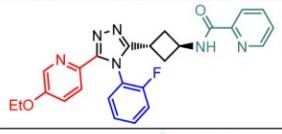	14	19	>80	40 / 0.6	<15 / >90	37 / 36
14	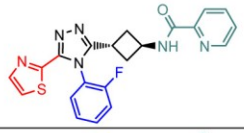	29	127				
15	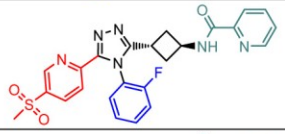	9.2	12			<15 / >90	<15 / >90
16 #	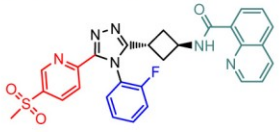	1.8	0.81	>36	14 / 2.9	<15 / >90	37 / 37

Table 1. Hybrids derived from **19** and **20**, **22** and three West-moieties. # indicates that these compounds were evaluated in a mouse pharmacokinetics analysis.

the South 2-chlorophenyl substituent, we analyzed all synthesized compounds with chiral SFC. All compounds with a South 2-chlorophenyl group showed atropisomers, while compounds without this group, including the symmetric 2,6-dichlorophenyl **67**, did not (Supplementary Table 1c). In addition, **66**, containing a bulky 2-trifluoromethyl group, also showed two signals on a chiral SFC column. No rotamers were observed for the 2-fluorophenyl South group at room temperature. Hence, this group was considered a viable substitution to avoid atropisomerism. As a consequence, in the following optimization campaign, the South 2-chlorophenyl moiety was replaced with the 2-fluorophenyl group of **23** resulting in acceptable efficacy compared to other substitutions (Figure 2a and Supplementary Table 1c).

The comparison of the binding modes of the 2-halogen-substituted compounds showed that the chlorine or fluorine atoms were pointing into the same direction in the TNKS2 active site (Figure 3 and Supplementary Figure 1b-e). This is in agreement with the clear difference in the measured potencies of the atropisomers (Figure 4). The South-moiety without a halogen was less potent, had similar orientation in the binding pocket, but caused a conformational change in the Tyr1050 covering the active site (Supplementary Figure 1d).

Next, all possible hybrid combinations were synthesized employing the East-moieties of compounds **20** and **21**, a South 2-fluorophenyl group and three different West-moieties revisiting the 2-pyridyl-4-methylsulphonyl moiety as well (Table 1).[9] From these six molecules, compounds with the 1,5-naphthyridine moiety (**10**, **11** and **12**) showed approximately 30-fold improved cellular inhibitory efficacy compared to their counterparts with the 2-pyridyl moiety (**13**, **14** and **15** respectively, Table 1). The binding mode of compound **13** in co-crystal structures was similar, and the hydrogen bonds to the backbone amides seen in the **1** co-crystal structures were retained (Figure 3 and Supplementary Figure 1b). The large East-moieties 1,5- and 1,6-naphthyridine (see e.g. **87**, **88**, **106** and **107** Supplementary Figure 4a) appeared to form a more efficient π-π-stacking interaction with His1048, and a hydrophobic interaction with Phe1035, causing the side chain to gradually rotate according to the form of the East-moiety (Figure 3c-d, Supplemen-

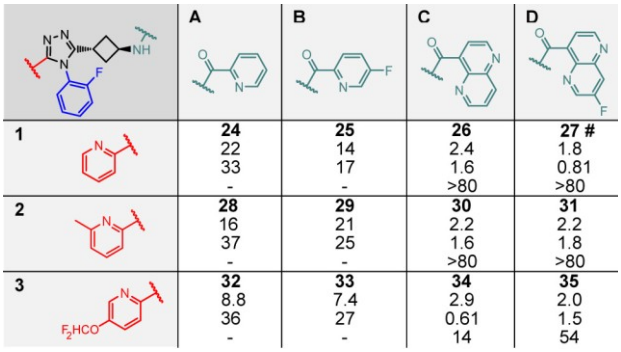

	A	B	C	D
1	**24** 22 33 -	**25** 14 17 -	**26** 2.4 1.6 >80	**27 #** 1.8 0.81 >80
2	**28** 16 37 -	**29** 21 25 -	**30** 2.2 1.6 >80	**31** 2.2 1.8 >80
3	**32** 8.8 36 -	**33** 7.4 27 -	**34** 2.9 0.61 14	**35** 2.0 1.5 54

Table 2. 2D East (green) and West library (red) with TNKS2 IC_{50} (nM), HEK293 IC_{50} (nM) and solubility (μM) values depicted. # indicates that the compound was evaluated in a mouse pharmacokinetics analysis.

tary Figure 1c-e, Supplementary Table 2). However, compounds with this naphthyridine moiety were less stable in microsomes relative to the corresponding East-pyridines, and consequently, **13** was shortlisted for mouse pharmacokinetics studies. In addition, the quinoline-containing **16** displayed similar inhibition in the cellular WNT reporter assay compared to **12,** and also possessed improved calculated phys-chem properties (ChemAxon: cLogP 3.0/3.7, tPSA 128/141 for **16** and **12** respectively)(Figure 2a and Table 1). Based on these results, **16** was shortlisted for mouse pharmacokinetics analysis. Further optimization focused on pyridine-type West-side variations and discarded the West 2-thiazole (**11**) because of adverse solubility and low efficacy (**14**) (Table 1). In an East and West 2D library, fluorinated analogues of the 2-pyridyl and the 1,5-naphthyridine were introduced (Table 2 and Supplementary Table 2). From these compounds, **27** was shortlisted for mouse pharmacokinetics analysis.

Compared to the initial benchmark lead compound **1,** the peroral mouse pharmacokinetics data of the selected and shortlisted compounds showed significantly improved profiles exhibiting lower clearance and volume of distribution and 15-35 times higher exposure (Figure 2c). On due course of the study, **13** had been further characterized including selectivity towards other members of the PARP family, structural analysis of its binding mode, kinetic solubility, Caco-2 permeability and efflux, CYP3A4 inhibition, mouse plasma stability, mouse plasma protein binding, hERG inhibition, Ames test and off-target safety panel, exhibiting overall favorable parameters (Figure 3, Table 3, Supplementary Table 3 and Supplementary Figure 2).

Tankyrase inhibition can context-dependently antagonize proliferation and viability in cancer cell lines *in vitro* and *in vivo*, including in the colorectal adenocarcinoma cell line COLO 320DM harboring WNT/β-catenin signaling-inducing *APC* mutations[5, 22]. Hence, cultured COLO 320DM cells were treated with various doses of **13** to evaluate the efficacy in reducing canonical WNT/β-catenin signaling and the potential as an anti-proliferative agent. As expected for a potent tankyrase inhibitor, treatment with **13** reduced TNKS1/2 protein levels, stabilized AXIN1 and AXIN2 proteins and reduced the level of transcriptionally active β-catenin (non-phoshorylated) in both the cytoplasmic and nuclear fraction (Figure 5a and Supplementary Figure 3a and b). Administration of **13** also decreased transcription of the WNT/β-catenin signaling target genes *AXIN2, DKK1, NKD1* and *APCDD1* (Figure 5b). Moreover, **13** exposure decreased proliferation and viability in COLO 320DM cells (GI50 = 650 nM and GI25 = 94 nM), while control $APC^{wild\text{-}type}$ RKO colorectal cancer cells were only modestly affected by the treatment at a 10 μM compound concentration (Figure 5c). In conclusion, these results authenticate that **13** can both potently and specifically inhibit WNT/β-catenin signaling activity and act as an anti-proliferative agent in COLO 320DM cells.

CONCLUSION

In summary, through a systematic building block-based and crystallography-guided structure-activity-relationship analysis, we identified novel 1,2,4-triazole-based optimized lead tankyrase inhibitors with low nanomolar and picomolar IC_{50} activities in a WNT/β-catenin signaling cellular reporter assay. The adverse chemical properties of the preceding lead compound **1**[11], displaying atropisomerism and solubility liabilities, were excluded in the here identified advanced lead compound **13.** Compound **13** shows high selectivity towards TNKS1/2, an overall favorable ADME, including highly improved Caco-2 permeability and microsomal stability,

Parameter	1	13
MW (g/mol)	468.91	458.50
ALogP (LiveDesign 8.6)	4.7	3.6
AlogD (LiveDesign 8.6)	5.3	4.0
tPSA (LiveDesign 8.6) (Å²)	118.1	94.8
TNKS1 (IC50, nM)	29	127
TNKS2 (IC50, nM)	6.3	14
PARPs/ARTDs (IC50, μM) ARTD1/2/3/4/7/8/10/12	>10	>10
HEK293 cells (IC50, nM)	19	19
Kinetic solubility: PBS pH=7 (μM)	12	95.7
Caco-2 A-B: P_{app} (10^{-6} cm/s)	10.0	39.5
Caco-2 efflux ratio	4.17	0.610
Microsomal stability human / mouse Cl_{int} (μl/min/mg protein)	242 / 204	<15 / 37
Hepatocyte stability human / mouse / dog / rat / cynomolgus: Cl_{int} (μl/min/10^6 cells)	9.8 / ND / ND / ND / ND	<0.1 / 28 / <0.1 / 3.8 / <0.1
CYP3A4 inhibition (IC50, μM)	1.26	> 25
Mouse plasma stability $t_{1/2}$ (min)		880
Mouse PPB (%)		93.92
hERG inhibition (IC50, μM)		> 25
Ames test		non-genotoxic
Cerep Safety panel 44 targets (10 μM)		clean (A2A, 53% inhib.)
Bioavailability F (%)	47	107
PO PK mouse $t_{1/2}$ (h)	1.5	0.67
PO PK mouse CL (L/h/Kg)	34.0	2.09
PO PK mouse Vd (L/Kg)	74.2	2.03
PO PK mouse AUC 0→t	145	2384

Table 3. Profiling of **1** and **13.** Not determined = ND.

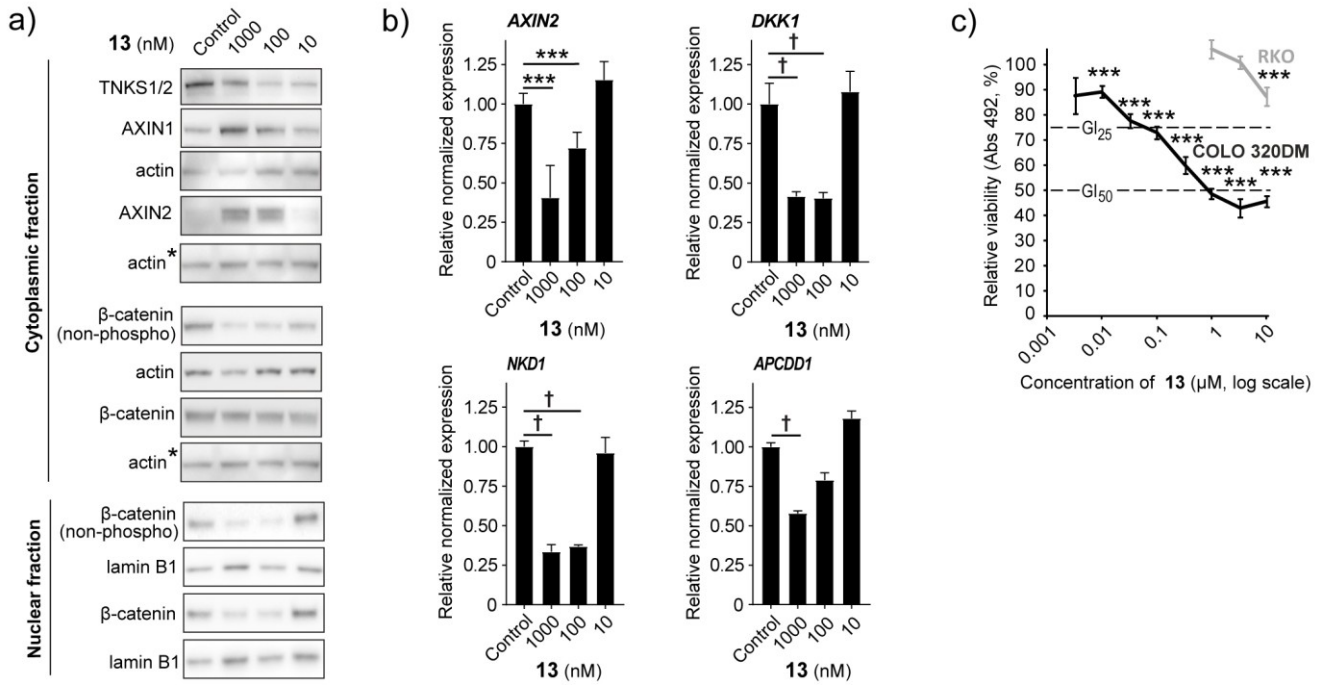

Figure 5. 13 can inhibit WNT/β-catenin signaling activity and act as an anti-proliferative agent in COLO 320DM cells. (a) Representative immunoblots of cytoplasmic TNKS1/2, AXIN1, AXIN2 and cytoplasmic and nuclear transcriptionally active β-catenin (non-phospho) and β-catenin. Actin or lamin B1 document equal protein loading and * indicates that the same actin immunoblot is used as loading control for both AXIN2 and β-catenin. For a and b, control = 0.01% DMSO. (b) Real-time RT-qPCR analyses of WNT/β-catenin signaling target genes (*AXIN2, DKK1, NKD1* and *APCDD1*). For (b) and (c): ANOVA tests (Holm-Sidak method, versus control) are indicated by *** ($P < 0.001$) and ANOVA on ranks tests (Tukeys test versus control) are indicated by $^{+}$ ($P < 0.05$). Mean values ± standard deviations for combined data from minimum 3 independent experiments with three replicates each are shown. (c) MTS colorimetric cell growth assay for various doses of 13 in $APC^{mutated}$ COLO 320DM (black) and $APC^{wild\text{-}type}$ RKO (grey) cells. Control = 0. 1% DMSO. Dotted lines depict 50% (GI_{50}) and 25% (GI_{25}) growth inhibition levels. Mean values ± standard deviations for one representative experiment out of three independent experiments are shown.

a clean off-target safety profile, a >15-fold increased exposure in a mouse pharmacokinetics analysis and a robust inhibition of WNT/β-catenin signaling and proliferation in the colon cancer cell line COLO 320DM. Our work provides a considerably optimized compound for targeting TNKS1/2 and WNT/β-catenin signaling in cancer and other disease models.

EXPERIMENTAL SECTION

General methods. All starting materials and dry solvents were commercially obtained. The synthesis of hydrazide **2** was scaled-up employing a similar procedure reported in our earlier publication.[11] Reactions were performed under an inert atmosphere of nitrogen, when necessary. Microwave reactions were carried out in sealed vials. Column chromatography was carried out on silica gel cartridges (40 um irregular) and TLC analysis was performed on silica gel 60 F_{254} plates.

NMR. NMR spectra were recorded in chloroform-d, unless otherwise stated, on a 400 MHz spectrometer with tetramethylsilane as internal standards. Coupling constants are given in Hz; peaks are reported as singlet (s), doublet (d), triplet (t), quartet (q), quintet (p), sextet (h), septet (hept), multiplet (m) or combination thereof; br stands for broad.

LC/MS. LC/MS chromatograms mass spectra were recorded using electrospray ionization in positive or negative ionization mode on Agilent 1260 Bin. Pump: G1312B, Degasser; Autosampler; ColCom; DAD G1315C; MSD G6130B ESI; Eluent A: acetonitrile, Eluent B: 10mM ammonium bicarbonate in water (base mode) or 0.1% formic acid in water (acid mode).

HRMS. HRMS spectra were recorded with a LC-MS Q Exactive Focus spectrometer calibrated with the Pierce calibration solution both in pos. and neg. mode.

GC/MS. Agilent 6890N, injection S/SL; Injector 7683 and MS: 5973 MS, EI-positive; Carrier gas He.

Analytical SFC. Waters UPC2, Bin pump ACQ-ccBSM; Autosampler, Column Manager; PDA ACQ-PDA; QDA and Isocratic pump ACQ-ISM; Eluent A: CO_2, Eluent B: MeOH + 20 mM ammonia.

Preparative SFC. Waters Prep 100 SFC UV/MS directed system; Waters 2998 Photodiode Array (PDA) Detector; Waters Acquity QDa MS detector; Waters 2767 Sample Manager; Columns: Phenomenex Lux Amylose-1 (250x21 mm, 5 μm), Phenomenex Lux Cellulose-1 (250x21.2 mm, 5 μm), Phenomenex Lux Cellulose-2 (250x21.2 mm, 5 μm), Diacel Chiralpak IC for SFC (250x20 mm, 5 μm); Column temp: 35°C; Flow: 70 mL/min; ABPR: 120 bar; Eluent A: CO2, Eluent B: 20 mM ammonia in methanol;

Linear gradient: t=0 min 10% B, t=5 min 50% B; t=7.5 min 50% B; Detection: PDA (210-400 nm); Fraction collection based on PDA TIC.

Analytical SFC. Waters UPC2, Bin pump ACQ-ccBSM; Autosampler, Column Manager; PDA ACQ-PDA; QDA and Isocratic pump ACQ-ISM. Phenomenex Amylose-1 (100x4.6 mm, 5 μm); Column temp: 35°C; Flow: 2.5 mL/min; BPR: 170 bar; Eluent A: CO2, Eluent B: MeOH + 20 mM Ammonia; Linear gradient: t=0 min 5% B, t=5 min 50% B; t=6 min 50% B; Detection: PDA (210-320 nm).

Reveleris MPLC. preparative base XSelect: Instrument type: Reveleris™ prep MPLC; column: Waters XSelect CSH C18 (145x25 mm, 10μ); Flow: 40 mL/min; Column temp: room temperature; Eluent A: 10 mM ammonium bicarbonate in water pH = 9.0); Eluent B: 99% acetonitrile + 1% 10 mM ammonium bicarbonate in water; Gradient: t=0 min 5% B, t=1 min 5% B, t=2 min 30% B, t=17 min 70% B, t=18 min 100% B, t=23 min 100% B; Detection UV: 220, 254, 340 nm.

Reveleris MPLC. preparative acid Luna: Instrument type: Reveleris™ prep MPLC; Column: Phenomenex Luna C18(3) (150x25 mm, 10 μ); Flow: 40 mL/min; Column temp: room temperature; Eluent A: 0.1% (v/v) formic acid in water, Eluent B: 0.1% (v/v) formic acid in acetonitrile; Gradient: t=0 min 5% B, t=1 min 5% B, t=2 min 30% B, t=17 min 70% B, t=18 min 100% B, t=23 min 100% B; Detection UV : 220, 254, 340 nm, ELSD.

All test compounds were found to be >95% pure by LCMS and H-NMR analysis. Intermediates in the synthesis were >95% pure unless stated otherwise.

3-(*trans*-3-(5-(5-ethoxypyridin-2-yl)-4-(2-fluorophenyl)-4H-1,2,4-triazol-3-yl)cyclobutyl)-1,5-naphthyridine-4-carboxamide (10). The title compound was prepared according to the general procedure F as a white solid (21.4 mg, 38% yield). LC/MS (ESI) m/z for $C_{28}H_{24}FN_7O_2$ 509 (calcd) 510 ([M+H]+, found). ^{1}H NMR (400 MHz, Chloroform-d) δ 11.31 (d, J = 5.9 Hz, 1H), 9.14 (d, J = 4.4 Hz, 1H), 8.98 (dd, J = 4.2, 1.8 Hz, 1H), 8.58 – 8.52 (m, 2H), 8.17 (d, J = 8.8 Hz, 1H), 7.88 (d, J = 2.9 Hz, 1H), 7.74 (dd, J = 8.6, 4.2 Hz, 1H), 7.48 – 7.40 (m, 1H), 7.26 – 7.14 (m, 4H), 4.84 (h, J = 6.9 Hz, 1H), 4.04 (q, J = 7.0 Hz, 2H), 3.53 (tt, J = 10.3, 5.6 Hz, 1H), 3.14 – 3.02 (m, 2H), 2.62 – 2.48 (m, 2H), 1.40 (t, J = 7.0 Hz, 3H).

3-(*trans*-3-(4-(2-fluorophenyl)-5-(thiazol-2-yl)-4H-1,2,4-triazol-3-yl)cyclobutyl)-1,5-naphthyridine-4-carboxamide (11). The title compound was prepared according to the general procedure F as a white solid (6.6 mg, 23% yield). LC/MS (ESI) m/z for $C_{24}H_{18}FN_7OS$ 471 (calcd) 472 ([M+H]+, found). ^{1}H NMR (400 MHz, Chloroform-d) δ 11.33 (d, J = 6.0 Hz, 1H), 9.15 (d, J = 4.5 Hz, 1H), 8.98 (dd, J = 4.2, 1.8 Hz, 1H), 8.59 – 8.52 (m, 2H), 7.75 (dd, J = 8.5, 4.2 Hz, 1H), 7.65 (d, J = 3.2 Hz, 1H), 7.57 – 7.47 (m, 1H), 7.37 (d, J = 3.2 Hz, 1H), 7.34 – 7.22 (m, 3H), 4.92 – 4.80 (m, 1H), 3.60 – 3.49 (m, 1H), 3.15 – 3.02 (m, 2H), 2.68 – 2.51 (m, 2H).

3-(*trans*-3-(4-(2-fluorophenyl)-5-(5-(methylsulfonyl)pyridin-2-yl)-4H-1,2,4-triazol-3-yl)cyclobutyl)-1,5-naphthyridine-4-carboxamide (12). The title compound was prepared according to the general procedure F as a white solid (14.8 mg, 53% yield). LC/MS (ESI) m/z for $C_{27}H_{22}FN_7O_3S$ 543 (calcd) 544 ([M+H]+ found). ^{1}H NMR (400 MHz, Chloroform-d) δ 11.31 (br d, J = 6.1 Hz, 1H), 9.15 (d, J = 4.5 Hz, 1H), 8.97 (dd, J = 4.2, 1.8 Hz, 1H), 8.73 (dd, J = 2.5, 0.8 Hz, 1H), 8.57 (pseudo d, J = 1.6 Hz, 1H), 8.55 (pseudo d, J = 4.2 Hz, 2H), 8.29 (dd, J = 8.3, 2.3 Hz, 1H), 7.74 (dd, J = 8.5, 4.2 Hz, 1H), 7.55 – 7.46 (m, 1H), 7.30 – 7.19 (m, 3H), 4.89 (h, J = 7.1 Hz, 1H), 3.55 (tt, J = 10.0, 5.5 Hz, 1H), 3.17 – 3.02 (m, 2H), 3.08 (s, 3H), 2.69 – 2.52 (m, 2H).

3-(*trans*-3-(5-(5-ethoxypyridin-2-yl)-4-(2-fluorophenyl)-4H-1,2,4-triazol-3-yl)cyclobutyl)picolinamide (13). The title compound was prepared according to the general procedure F as a white solid (16.8 mg, 46% yield). LC/MS (ESI) m/z for $C_{25}H_{23}FN_6O_2$ = 458 (calculated), 459 ([M+H]$^+$, found). ^{1}H NMR (400 MHz, chloroform-d) δ 8.53 (dt, J = 4.7, 1.3 Hz, 1H), 8.21 (d, J = 7.0 Hz, 1H), 8.19 – 8.12 (m, 2H), 7.88 (d, J = 2.8 Hz, 1H), 7.83 (td, J = 7.7, 1.7 Hz, 1H), 7.48 – 7.38 (m, 2H), 7.24 – 7.15 (m, 4H), 4.76 (h, J = 7.0 Hz, 1H), 4.04 (q, J = 6.9 Hz, 2H), 3.47 (tt, J = 10.0, 5.1 Hz, 1H), 3.09 – 2.97 (m, 2H), 2.52 – 2.36 (m, 2H), 1.40 (t, J = 7.0 Hz, 3H). HRMS 459.19393 ([M+H]$^+$, calculated), 459.19353 ([M+H]$^+$, found), Δ = -0.87 ppm.

3-(*trans*-3-(4-(2-fluorophenyl)-5-(thiazol-2-yl)-4H-1,2,4-triazol-3-yl)cyclobutyl)picolinamide (14). The title compound was prepared according to the general procedure F as a white solid (21.3 mg, 84% yield). LC/MS (ESI) m/z for $C_{21}H_{17}FN_6OS$ 420 (calcd) 421 ([M+H]+, found). ^{1}H NMR (400 MHz, Chloroform-d) δ 8.53 (dq, J = 4.5, 0.9 Hz, 1H), 8.23 (br d, J = 7.0 Hz, 1H), 8.17 (dt, J = 7.8, 1.1 Hz, 1H), 7.84 (td, J = 7.7, 1.7 Hz, 1H), 7.64 (d, J = 3.2 Hz, 1H), 7.57 – 7.49 (m, 1H), 7.43 (ddd, J = 7.8, 4.7, 1.3 Hz, 1H), 7.37 (d, J = 3.2 Hz, 1H), 7.33 – 7.27 (m, 2H), 7.26 – 7.21 (m, 1H), 4.78 (h, J = 7.0 Hz, 1H), 3.54 – 3.43 (m, 1H), 3.11 – 2.96 (m, 2H), 2.56 – 2.39 (m, 2H). HRMS 421.12413 ([M+H]$^+$, calculated), 421.12330 ([M+H]$^+$, found), Δ = -0.84 ppm.

3-(*trans*-3-(4-(2-fluorophenyl)-5-(5-(methylsulfonyl)pyridin-2-yl)-4H-1,2,4-triazol-3-yl)cyclobutyl)picolinamide (15). The title compound was prepared according to the general procedure F as a white solid (6.1 mg, 40% yield). LC/MS (ESI) m/z for $C_{24}H_{21}FN_6O_3S$ 492 (calcd) 493 ([M+H]+ found). ^{1}H NMR (400 MHz, Chloroform-d) δ 8.72 (d, J = 2.3 Hz, 1H), 8.58 – 8.51 (m, 2H), 8.28 (dd, J = 8.4, 2.3 Hz, 1H), 8.23 (br d, J = 7.0 Hz, 1H), 8.17 (dt, J = 7.7, 1.1 Hz, 1H), 7.84 (td, J = 7.7, 1.7 Hz, 1H), 7.55 – 7.47 (m, 1H), 7.43 (ddd, J = 7.6, 4.8, 1.2 Hz, 1H), 7.29 – 7.17 (m, 3H), 4.80 (h, J = 7.1 Hz, 1H), 3.53 – 3.44 (m, 1H), 3.07 (s, 3H), 3.14 – 2.97 (m, 2H), 2.57 – 2.40 (m, 2H).

3-(*trans*-3-(4-(2-fluorophenyl)-5-(5-(methylsulfonyl)pyridin-2-yl)-4H-1,2,4-triazol-3-yl)cyclobutyl)quinoline-8-carboxamide (16). The title compound was prepared according to the general procedure F as a white solid (24.9 mg, 91% yield). LC/MS (ESI) m/z for $C_{28}H_{23}FN_6O_3S$ = 542 (calculated), 543 ([M+H]$^+$ found). ^{1}H NMR (400 MHz, chloroform-d) δ 11.56 (d, J = 5.8 Hz, 1H), 8.91 (dd, J = 4.3, 1.8 Hz, 1H), 8.83 (dd, J = 7.4, 1.6 Hz, 1H), 8.73 (d, J = 2.3 Hz, 1H), 8.56 (d, J = 8.4 Hz, 1H), 8.28 (dt, J = 8.4, 2.5 Hz, 2H), 7.96 (dd, J = 8.1, 1.6 Hz, 1H), 7.67 (t, J = 7.7 Hz, 1H), 7.49 (dt, J = 8.3, 5.0 Hz, 2H), 7.26 – 7.18 (m, 3H), 4.85 (apparent dq, J = 13.4, 6.8 Hz, 1H), 3.57 (apparent tt, J = 10.1, 5.8 Hz, 1H), 3.16 – 3.01 (m, 2H), 3.08 (s, 3H), 2.67 – 2.50 (m, 2H). HRMS 543.16091 ([M+H]$^+$, calculated), 543.16007 ([M+H]$^+$, found), Δ = -0.84 ppm.

3-(*trans*-3-(4-(2-chlorophenyl)-5-(pyrimidin-4-yl)-4H-1,2,4-triazol-3-yl)cyclobutyl)-2-oxo-2,3-dihydrobenzo[d]oxazole-6-carbonitrile (18). Crude hydroxybenzonitrile (**8**) (10 mg, 0.014 mmol, ~60% pure) was dissolved in DCM (dried, 3.0 mL) under a nitrogen atmosphere. Acetonitrile (anhydrous, 1.0 mL) was also added followed by CDI (11 mg, 0.070 mmol) and the mixture was stirred for 60 hours at ambient temperature. The solvent was evaporated and the residue was purified by preparative SFC. After freeze-drying the purified fractions from acetonitrile / water, 2.8 mg (42% yield) of a white powder of the target compound (**18**) was obtained. LC/MS (ESI) m/z for $C_{24}H_{16}ClN_7O_2$ = 469 / 471 (calculated), 470 / 472 ([M+H]$^+$, found). ^{1}H NMR (400 MHz, chloroform-d) δ 8.86 – 8.82 (m, 2H), 8.28 (dd, J = 5.3, 1.2 Hz, 1H), 7.60 – 7.50 (m, 3H), 7.51 – 7.42 (m, 2H), 7.30 (dd, J = 7.8, 1.4 Hz, 1H), 7.18 (d, J = 8.2 Hz, 1H), 5.20 (p, J = 8.3 Hz, 1H), 3.44 – 3.34 (m, 2H), 3.34 – 3.25 (m, 1H), 2.98 (td, J = 8.5, 4.1 Hz, 1H), 2.93 – 2.83 (m, 1H).

1-(3-(4-(2-chlorophenyl)-5-(pyrimidin-4-yl)-4H-1,2,4-triazol-3-yl)bicyclo[1.1.1]pentan-1-yl)-2-oxo-2,3-dihydro-1H-benzo[d]imidazole-5-carbonitrile (19). Under a nitrogen atmosphere an impure batch of 3-amino-4-((3-(4-(2-chlorophenyl)-5-(pyrimidin-4-yl)-4H-1,2,4-triazol-3-yl)bicyclo[1.1.1]pentan-1-yl)amino)benzonitrile **19b** (36 mg, 0.060 mmol, ~75% pure, see supporting information) was dissolved in dry DCM (6.0 mL) and it was treated at ambient temperature with several portions of CDI (in total 9 equiv.) over a period of 24 hours till the complete conversion was reached. The mixture was evaporated to dryness and the residue was first flashed on a 12 gram silica gel cartridge eluted with a gradient of methanol (0% via 3% to 10%) in DCM. Then it was submitted to purification by preparative SFC isolating 19.0 mg (65% yield) of a white powder. LC/MS (ESI) m/z for $C_{25}H_{17}ClN_8O$ = 480 / 482 (calculated), 481 / 483 ([M+H]$^+$, found). ^{1}H NMR (400 MHz, DMSO-d6) δ 11.36 (s, 1H), 8.95 (d, J = 5.3 Hz, 1H), 8.90 (d, J = 1.2 Hz, 1H), 8.23 (dd, J = 5.3, 1.3 Hz, 1H), 7.79 (dd, J = 7.8, 1.5 Hz, 1H), 7.76 (dd, J = 8.0, 1.2 Hz, 1H), 7.66 (td, J = 7.8, 1.6 Hz, 1H), 7.58 (td, J = 7.6, 1.3 Hz, 1H), 7.44 (dd, J = 8.3, 1.4 Hz, 1H), 7.40 – 7.30 (m, 2H), 2.61 – 2.52 (m – distorted q, 6H). HRMS 481.12866 ([M+H]$^+$, calculated), 481.12796 ([M+H]$^+$, found), Δ = -1.46 ppm.

3-(*trans*-3-(4-(2-chlorophenyl)-5-(pyrimidin-4-yl)-4H-1,2,4-triazol-3-yl)cyclobutyl)picolinamide (20). The title compound was prepared according to the general procedure F and obtained as a white solid (41.1 mg, 94% yield). LC/MS (ESI) m/z for $C_{22}H_{18}ClN_7O$ = 431 / 433 (calculated), 432 / 434 ([M+H]$^+$, found). ^{1}H NMR (400 MHz, chloroform-d) δ 8.82 (s, 1H), 8.81 (d, J = 3.3 Hz, 1H), 8.53 (qd, J = 4.8, 0.6 Hz, 1H), 8.28 (dd, J = 5.3, 1.3 Hz, 1H), 8.23 (d, J = 6.6 Hz, 1H), 8.17 (d, J = 7.8 Hz, 1H), 7.84 (td, J = 7.7, 1.7 Hz, 1H), 7.54 (dd, J = 8.0, 1.5 Hz, 1H), 7.49 (td, J = 7.7, 1.6 Hz, 1H), 7.46 – 7.38 (m, 2H), 7.30 (dd, J = 7.8, 1.5 Hz, 1H), 4.86 – 4.72 (m, 1H), 3.49 – 3.36 (m, 1H), 3.11 – 3.00 (m, 2H), 2.53 – 2.38 (m, 2H). HRMS 432.13341 ([M+H]$^+$, calculated), 432.13272 ([M+H]$^+$, found), Δ = -1.61 ppm.

3-(*trans*-3-(4-(2-chlorophenyl)-5-(pyrimidin-4-yl)-4H-1,2,4-triazol-3-yl)cyclobutyl)-1,5-naphthyridine-4-carboxamide (21). The title compound was prepared according to the general procedure F and obtained as a white solid (12.7 mg, 26% yield). LC/MS (ESI) m/z for $C_{25}H_{19}ClN_8O$ = 482 / 484 (calculated), 483 / 485 ([M+H]$^+$, found). ^{1}H NMR (400 MHz, chloroform-d) δ 11.32 (d, J = 5.8 Hz, 1H), 9.15 (d, J = 4.4 Hz, 1H), 8.98 (dd, J = 4.2, 1.7 Hz, 1H), 8.85 – 8.79 (m, 2H), 8.60 – 8.52 (m, 2H), 8.29 (dd, J = 5.3, 1.3 Hz, 1H), 7.75 (dd, J = 8.5, 4.2 Hz, 1H), 7.54 (dd, J = 7.9, 1.5 Hz, 1H), 7.48 (td, J = 7.7, 1.6 Hz, 1H), 7.42 (td, J = 7.6, 1.6 Hz, 1H), 7.32 (dd, J = 7.8, 1.5 Hz, 1H), 4.88 (h, J = 7.2 Hz, 1H), 3.49 (tt, J = 9.7, 5.4 Hz, 1H), 3.17 – 3.04 (m, 2H), 2.65 – 2.50 (m, 2H). HRMS 483.14431 ([M+H]$^+$, calculated), 483.14350 ([M+H]$^+$, found), Δ = -0.81 ppm.

3-(*trans*-3-(4-(2-chlorophenyl)-5-(5-ethoxypyridin-2-yl)-4H-1,2,4-triazol-3-yl)cyclobutyl)-2-oxo-2,3-dihydro-1H-benzo[d]imidazole-5-carbonitrile (22). The title compound was prepared according to the General Procedure D from (1r,3r)-3-(5-cyano-2-oxo-2,3-dihydro-1H-benzo[d]imidazol-1-yl)cyclobutane-1-carbohydrazide **2**[11] (60.2 mg, 0.222 mmol) and methyl *N*-(2-chlorophenyl)-5-ethoxypyridine-2-carbimidothioate **E2** (68 mg, 0.222 mmol) affording 49.9 mg (42% yield) of a white solid. LC/MS (ESI) m/z for $C_{27}H_{22}ClN_7O_2$ = 511 (calculated), 512 ([M+H]$^+$, found). ^{1}H NMR (400 MHz, chloroform-d) δ 8.69 (s, 1H), 8.17 (d, J = 8.8 Hz, 1H), 7.87 (d, J = 2.8 Hz, 1H), 7.51 (distorted dd, J = 7.8, 1.8 Hz, 1H), 7.46 (td, J = 7.6, 1.8 Hz, 1H), 7.44 – 7.38 (m, 2H), 7.31 (distorted dd, J = 7.7, 1.7 Hz, 2H), 7.25 – 7.18 (m, 2H), 5.28 (t, J = 8.4 Hz, 1H), 4.04 (q, J = 7.0 Hz, 2H), 3.45 – 3.29 (m, 3H), 3.00 – 2.84 (m, 2H), 1.40 (t, J = 7.0 Hz, 3H). HRMS 512.15963 ([M+H]$^+$, calculated), 512.15900 ([M+H]$^+$, found), Δ = -1.23 ppm.

3-(*trans*-3-(4-(2-fluorophenyl)-5-(pyrimidin-4-yl)-4H-1,2,4-triazol-3-yl)cyclobutyl)-2-oxo-2,3-dihydro-1H-benzo[d]imidazole-5-carbonitrile (23). The title compound was prepared according to the general procedure D from (1r,3r)-3-(5-cyano-2-oxo-2,3-dihydro-1H-benzo[d]imidazol-1-yl)cyclobutane-1-carbohydrazide **2**[11] (43.9 mg, 0.162 mmol) and methyl *N*-(2-fluorophenyl)pyrimidine-4-carbimidothioate **E3** (40 mg, 0.162 mmol) as a white powder (14 mg, 19% yield). LC/MS (ESI) m/z for $C_{24}H_{17}FN_8O$ = 452 (calculated), 453 ([M+H]$^+$, found). ^{1}H NMR (400 MHz, chloroform-d) δ 8.87 (d, J = 1.4 Hz, 1H), 8.85 (d, J = 5.2 Hz, 1H), 8.71 (br s, 1H), 8.29 (dd, J = 5.3, 1.4 Hz, 1H), 7.61 – 7.53 (m, 1H), 7.43 (dd, J = 8.3, 1.5 Hz, 1H), 7.35 – 7.29 (m, 2H), 7.26 – 7.22 (m, 2H), 7.19 (d, J = 8.3 Hz, 1H), 5.27 (p, J = 8.7 Hz, 1H), 3.54 – 3.44 (m, 2H), 3.39 (apparent q, J = 10.3 Hz, 1H), 3.05 – 2.97 (m, 1H), 2.88 – 2.78 (m, 1H). HRMS 453.15821 ([M+H]$^+$, calculated), 453.15769 ([M+H]$^+$, found), Δ = -1.16 ppm.

3-(*trans*-3-(4-(2-fluorophenyl)-5-(pyridin-2-yl)-4H-1,2,4-triazol-3-yl)cyclobutyl)-7-fluoro--1,5-naphthyridine-4-carboxamide (27). The title compound was prepared according to the general procedure F as a white solid (17.2 mg, 70% yield). LC/MS (ESI) m/z for $C_{26}H_{19}F_2N_7O$ = 483 (calculated), 484 ([M+H]$^+$, found). 1H NMR (400 MHz, chloroform-d) δ 10.83 (d, J = 6.0 Hz, 1H), 9.15 (d, J = 4.5 Hz, 1H), 8.91 (d, J = 2.8 Hz, 1H), 8.52 (d, J = 4.4 Hz, 1H), 8.26 (dt, J = 7.9, 1.0 Hz, 1H), 8.24 – 8.16 (m, 2H), 7.77 (td, J = 7.8, 1.8 Hz, 1H), 7.50 – 7.42 (m, 1H), 7.25 – 7.15 (m, 4H), 4.87 (ht, J = 6.8, 1.6 Hz, 1H), 3.53 (tt, J = 9.3, 5.6 Hz, 1H), 3.15 – 3.02 (sym. m, 2H), 2.63 – 2.47 (sym. m, 2H). HRMS

484.16919 ([M+H]$^+$, calculated), 484.16833 ([M+H]$^+$, found), Δ = -1.78 ppm.

Preparation of 3-(*trans*-3-(4-(2-chlorophenyl)-5-(pyrimidin-4-yl)-4H-1,2,4-triazol-3-yl)cyclobutyl)isoindolin-1-one (51). 2-formylbenzoic acid (**9**) (33 mg, 0.22 mmol) was suspended in DCM (dry, 1.0 mL) under a nitrogen atmosphere and a solution of *trans*-3-(4-(2-chlorophenyl)-5-(pyrimidin-4-yl)-4H-1,2,4-triazol-3-yl)cyclobutan-1-amine (**Ga**) (0.20 mmol) in acetonitrile (anhydrous, 1.0 mL) and acetic acid (13 µl, 0.22 mmol) were added. The resulting solution was stirred for 17 hours at ambient temperature. Then, two portions of sodium triacetoxyborohydride (each of 85 mg, 0.40 mmol) were added and the was stirred for 3 hours at ambient temperature. Extra methanol was added (extra dry, 1.0 mL) for better dissolution. The mixture was then heated at 50 °C overnight for 40 hours while two extra portions of sodium triacetoxyborohydride were added (each of 85 mg, 0.40 mmol). The mixture was evaporated to dryness and the residue was quenched with water and a few mL of 1 N aqueous HCl. DCM was added, the aqueous phase was basified with aqueous sodium bicarbonate, and the crude product was extracted with DCM (three times). The extracts were dried over sodium sulphate, filtered and evaporated to dryness. The crude material was purified on a 12 gram silica gel cartridge eluted with a gradient of methanol (0% to 5%) in DCM. The product fraction was lyophilised from acetonitrile/water providing a white powder (34.1 mg, 38% yield) of the target compound. LC/MS (ESI) m/z for $C_{24}H_{19}ClN_6O$ = 442 / 444 (calculated) 443 / 445 ([M+H]$^+$, found). ^{1}H NMR (400 MHz, chloroform-d) δ 8.86 – 8.78 (m, 2H), 8.29 (dd, J = 5.3, 1.2 Hz, 1H), 7.81 (d, J = 7.4 Hz, 1H), 7.58 – 7.47 (m, 3H), 7.47 – 7.39 (m, 3H), 5.09 (p, J = 8.2 Hz, 1H), 4.44 (s, 2H), 3.42 – 3.31 (m, 1H), 2.98 – 2.80 (m, 4H).

Separation of atropisomers of 1 and investigation of their interconversion. An amount of 40 mg of racemic **1**[11] (40 mg, 0.085 mmol) was separated into pure atropisomers by preparative chiral SFC (see supporting information) providing respectively, 16.1 and 11.8 mg of off-white solids. Two sets of two samples dissolved in an acetonitrile / methanol mixture were prepared for each atropisomers. One set was heated in a reaction block at 70 °C, while the other was kept at ambient temperature. Samples were analysed after 24, 48 and 72 hours to check for the interconversion of atropisomers. After 24 hours no interconversion was observed at ambient temperature, while at 70 °C 2.5% of the opposite isomers was detected in both samples. After 48 hours of heating about 5-6% interconversion was observed at 70 °C. After 72 hours, the isomers showed no interconversion at ambient temperature, whereas at 70 °C about 8-9% of the other atropisomer was observed by chiral SFC.

Biochemical assays. Human tankyrase active constructs for TNKS1 (residues 1030-1317) and TNKS2 (residues 873-1162) and other ARTD/PARP enzymes used in the assays were expressed and purified as previously described.[34, 35] The enzymatic assay is based on the measurement of unreacted NAD$^+$, which is chemically converted into a fluorescent compound.[36] The fluorescence intensity was measured with excitation/emission wavelengths of 372 nm and 444 nm, respectively, using Tecan Infinity M1000 Pro. The compounds were prepared in half log dilution series and the reactions were done in quadruplicates with protein and compound controls to exclude the effect of compound auto-fluorescence. All reactions were done at ambient temperature. 20 nM of TNKS1 or 5 nM of TNKS2 were incubated for 20 hours in assay buffer (50 mM BTP pH 7.0, 0.5 mM TCEP, 0.01% Triton-X100) with compound and 10 µM or 500 nM NAD$^+$, respectively. 5 nM ARTD1/PARP1 or 20 nM ARTD2/PARP2 were incubated for 30 min with compound and 500 nM NAD$^+$ in assay buffer (50 mM Tris pH 8.0, 5 mM $MgCl_2$, 10 µg/ml activated DNA) supplemented with 0.2 or 0.1 mg/ml BSA, respectively. For ARTD3/PARP3, 20 nM of enzyme were incubated for 4 hours with compound and 500 nM NAD$^+$ in assay buffer (50 mM PIPES pH 7.0, 5 mM $MgCl_2$, 20 µg/ml activated DNA, 0.2 mg/ml BSA). The assay conditions for the other ARTD enzymes were used as previously described.[37]

WNT/β-catenin in signaling reporter assay. The luciferase-based WNT/β-catenin signaling pathway reporter assay in human HEK293 cells, as well as IC_{50} and GI_{50}/GI_{25} calculations, were performed as previously described.[9]

In vitro ADME assays. Kinetic solubility assay was performed following standard protocols of Mercachem. The following assays were performed according to the standard protocols of Cyprotex: Caco-2 permeability, dog microsomal stability, hepatocyte stability (human, mouse, dog, rat and cynomolgus), CYP3A4 inhibition, mouse plasma stability, mouse plasma protein binding and Ames test.

Microsomal Stability assay. Test compounds in DMSO (10 mM) were further diluted to 100 µM in acetonitrile. Human or mouse liver microsomes (BioIVT) from selected species are incubated in duplicate with the test compound at a final concentration of 1 µM in 0.1 M potassium phosphate buffer (pH 7.4) containing 3.3 mM MgCl2, 0.5 mg/ml microsomal protein, in the presence or absence of NADPH (1 mM). Incubations were performed at 37 °C in a total volume of 500 µl. Control incubations with reference substances were included for each experiment. At t = 0, 5, 15, 30, 45 min, 50 µl of the incubation mixture were transferred to a quench plate containing acetonitrile and internal standard (200 nM labetalol) cooled at 4 °C. After the last time point, the quench plates are mixed thoroughly and centrifuged for 15 minutes at 3700 rpm and 10 °C (Eppendorf 5804R). The supernatant was transferred to a 96 well plate and analyzed by LCMS (Vanquish Horizon UHPLC equipped with a diode array detector coupled to a Q Exactive focus hybrid quadrupole-Orbitrap mass spectrometer). The metabolic stability is evaluated by plotting the natural logarithm of the percentage test compound remaining versus time and performing linear regression.

Safety panel and hERG inhibition. Inhibition of 44 selected targets (n=2) including hERG (SafetyScreen 44) using 10 µM **13** was performed by Eurofins (Cerep-Panlabs).

Mouse pharmacokinetical analysis. The pharmacokinetical analyzes in mice were performed according to the standard protocols of Medicilon, and as previously described,[9] using 3 animals per treatment group using 5% DMSO, 50% PEG400 (both Sigma Aldrich) and 45% saline as vehicle.

Crystallography. Compounds **105**, **13**, **10**, **106**, **107**, **87**, **88** (Supplementary Table 4) were co-crystallized with the catalytic

domain of human TNKS2 (residues 952-1161) in the presence of chymotrypsin (1:100) based on crystallization efforts previously described.[11, 20] Protein (0.2 mM, 5.6 mg/ml) was mixed with 0.4 mM of compound from a 10 mM DMSO stock solution. The crystallization was set up at 22°C using sitting-drop vapor diffusion method by mixing 200 nl of protein with 100 nl of precipitant solution (0.1 M Bicine pH 8.5-9.0, 7.5-25% PEG6000). Rod-shaped crystals appeared within 24 hours and were cryoprotected using the precipitant solution containing 25% PEG6000 and 20% glycerol. Data were collected at ESRF Grenoble on beamlines ID30B, ID23-1 and ID30A-1 or at Diamond Light Source on beamline I04. Diffraction data was processed using the XDS package.[38] All structures were solved using molecular replacement with PHASER[39] using the structure of TNKS2 (PDB code: 5NOB) as a starting model. Coot[40] and Refmac5[41] were used for model building and refinement, respectively. The images of the structures were prepared using PyMOL (The PyMOL Molecular Graphics System, Version 1.8.4.0 Schrödinger, LLC.).

Western blot analysis. Western blot analysis of nuclear and cytoplasmic lysates from compound-treated COLO 320DM cells was performed as previously described[26] using the following primary antibodies: Tankyrase-1/2 (TNKS1/2, E-10, sc-365897, Santa Cruz Biotechnology), AXIN1 (C7B12, 3323, Cell Signaling Technology), AXIN2 (76G6, 2151, Cell Signaling Technology), non-phospho (active) β-catenin (D13A1, 8814, Cell Signaling Technology), β-catenin (610153,1:500, BD Biosciences). Actin (A2066, Sigma Aldrich) and lamin B1 (ab16048, Abcam) were used as loading controls. Primary antibodies were visualized with HRP-conjugated secondary antibodies (mouse anti-rabbit IgG, sc-2357, Santa Cruz Biotechnology or donkey anti-rabbit IgG, 711-035-152, Jackson ImmunoResearch) using ChemiDoc™ Touch Imaging System (Bio-Rad).

RNA isolation and real-time qRT-PCR. RNA isolation and real-time qRT-PCR was performed as previously described[26] using the following probes (all from Applied Biosystems): AXIN2 (Hs00610344_m1), DKK1 (Hs00183740_m1), NKD1 (Hs01548773_m1), APCDD1 (Hs00537787_m1) and GAPDH (Hs02758991_g1).

Proliferation assay. 1000 COLO 320DM cells per well were seeded in 96-well plates. The day after, cell culture medium was changed to contain various doses of **13** (n =4) or vehicle (DMSO, Sigma Aldrich) and the plates were incubated at 37 °C for 5 days. The cells were incubated for 1 hour at 37 °C with CellTiter 96® AQueous Non-Radioactive Cell Proliferation Assay (MTS, Promega) according to the supplier's recommendations. Abs_{490} was measured (Wallac 1420 Victor2 Microplate Reader, Perkin Elmer) and compared to Abs_{490} (t_0) using the following formula to determine single well values relative to the DMSO vehicle control: (sample A_{490} - average A_{490} t_0)×100/ (average A_{490} [for 0.01% DMSO controls] - average A_{490} t_0).

ASSOCIATED CONTENT

Supporting Information

The Supporting Information is available free of charge on the ACS Publications website. It contains general and specific synthetic procedure, additional figures and tables for inhibition data and crystallography (PDF).

Accession codes

Atomic coordinates and structure factors have been deposited to Protein Data Bank with accession codes 6TG4, 6TKM, 6TKN, 6TKP, 6TKQ, 6TKR, 6TKS.

AUTHOR INFORMATION

Corresponding Author

* jo.waaler@rr-research.no. Phone: +47 23 07 90 14

Author Contributions

The manuscript was written through contributions of all authors and all authors have given approval to the final version of the manuscript. # J.W., R.G.G.L. and S.T.S. contributed equally.

Funding Sources

J.W. and S.K. were supported by the Research Council of Norway (grant No. 262613, 267639 and 296226), by South-Eastern Norway Regional Health Authority (grant No. 16/00528-9, 15/00779-2, 2015012 and 2019090) and from the Norwegian Cancer Society (grant No. 5803958). L.L., S.T.S., A.G.-P. and S.M. were supported by the Jane and Aatos Erkko Foundation, Sigrid Jusélius Foundation and Academy of Finland (grant No. 287063, 294085 and 319299).

Notes

J.W., M.N., L.L., A.W., R.G.G.L. and S.K., hold patents related to tankyrase inhibitor therapy and these authors declare no additional interests. The remaining authors declare no competing interests.

ACKNOWLEDGMENT

Heli Alanen and Dr. Yves Nkizinkiko are acknowledged for their contribution in performing some of the biochemical assays. Ilonka Meerts[§] and Eef van den Elzen[§] are acknowledged for their contribution with the human and mouse microsomal stability assay. Protein crystallography experiments were performed at the Diamond Light Source (Didcot, UK) on beamline I04, and at European Synchrotron Radiation Facility (ESRF, Grenoble, France) on beamlines ID30B, ID23-1 and ID30A-1. We are grateful to Local Contacts for providing assistance in using the beamlines. The use of the facilities and expertise of the Biocenter Oulu Protein Crystallography core facility, a member of Biocenter Finland and Instruct-FI, is gratefully acknowledged.

ABBREVIATIONS

ADME, absorption, distribution, metabolism, and excretion; ADP, adenosine 5'-diphosphate; AKT serine/threonine kinase; AMOT, angiomotin; AMP, adenosine monophosphate; AMPK, AMP-activated protein kinase; APC, adenomatous polyposis coli; APCDD1, APC down-regulated 1; ARTD, Diphtheria toxin-like ADP-ribosyltransferase; AT, atropisomer; AUC, area under the curve; AXIN, axis inhibition protein; Boc, meaning *tert*-butyloxycarbonyl; CDI, *N*,*N*'-carbonyldiimidazole; CL, clearance; DIPEA, diisopropul ethylamine; DKK1, dickkopf WNT signaling pathway inhibitor 1; DMA, *N*,*N*-dimethyl acetamide; DMF, *N*,*N*-dimethyl formamide; DMSO, dimethyl sulfoxide; EGFR, epidermal growth factor receptor; equiv., equivalents; GSK3β, glycogen synthase kinase 3 beta; HATU, hexafluorophosphate azabenzotriazole tetramethyl uronium; HEK293, human embryonic kidney 293; hERG, human ether-à-go-go-related gene; HPLC, high pressure liquid chromatography; LATS1/2, large tumor sup-

pressor kinase 1 and 2; LC/MS, liquid chromatography / mass spectroscopy; MPLC, medium pressure liquid chromatography; MRT, mean residence time; MTS, 3-(4,5-dimethylthiazol-2-yl)-5-(3-carboxymethoxyphenyl)-2-(4-sulfophenyl)-2H-tetrazolium; NKD1, NKD inhibitor of WNT signaling pathway 1; NAD, nicotinamide adenine dinucleotide; NMR, nuclear magnetic resonance; PARP, poly-ADP-ribose polymerase; PARsylate, poly(ADP-ribose)sylate; PDA, photodiode array; PI3K, phosphoinositide-3-kinase; PK, pharmacokinetics; PO, per oral; PPB, plasma protein binding; Real-time RT-qPCR, real-time reverse transcription quantitative polymerase chain reaction; RNF146, ring finger protein 146; SD, standard deviation; SFC supercritical fluid chromatography; $t_{1/2,}$ half-life; TAZ, tafazzin; TEAD, TEA domain transcription factor; TFA, trifluoro acetic acid; TLC, thin layer chromatography; TNKS, telomeric repeat factor (TRF1)-interacting ankyrin-related ADP-ribose polymerases, tankyrase; TNKS1/2, tankyrase 1 and tankyrase 2; tPSA, total polar surface area; Vd, volume of distribution; WNT, Wingless-type mammary tumor virus integration site; YAP, yes associated protein 1.

REFERENCES

1. Haikarainen, T.; Krauss, S.; Lehtio, L. Tankyrases: structure, function and therapeutic implications in cancer. *Curr Pharm Des* **2014,** 20, 6472-6488.
2. Huang, S. M.; Mishina, Y. M.; Liu, S.; Cheung, A.; Stegmeier, F.; Michaud, G. A.; Charlat, O.; Wiellette, E.; Zhang, Y.; Wiessner, S.; Hild, M.; Shi, X.; Wilson, C. J.; Mickanin, C.; Myer, V.; Fazal, A.; Tomlinson, R.; Serluca, F.; Shao, W.; Cheng, H.; Shultz, M.; Rau, C.; Schirle, M.; Schlegl, J.; Ghidelli, S.; Fawell, S.; Lu, C.; Curtis, D.; Kirschner, M. W.; Lengauer, C.; Finan, P. M.; Tallarico, J. A.; Bouwmeester, T.; Porter, J. A.; Bauer, A.; Cong, F. Tankyrase inhibition stabilizes axin and antagonizes Wnt signalling. *Nature* **2009,** 461, 614-620.
3. Wang, W.; Li, N.; Li, X.; Tran, M. K.; Han, X.; Chen, J. Tankyrase inhibitors target YAP by stabilizing angiomotin family proteins. *Cell Rep* **2015,** 13, 524-532.
4. Bhardwaj, A.; Yang, Y.; Ueberheide, B.; Smith, S. Whole proteome analysis of human tankyrase knockout cells reveals targets of tankyrase-mediated degradation. *Nat Commun* **2017,** 8, 2214.
5. Kim, M. K. Novel insight into the function of tankyrase. *Oncol Lett* **2018,** 16, 6895-6902.
6. Li, N.; Wang, Y.; Neri, S.; Zhen, Y.; Fong, L. W. R.; Qiao, Y.; Li, X.; Chen, Z.; Stephan, C.; Deng, W.; Ye, R.; Jiang, W.; Zhang, S.; Yu, Y.; Hung, M. C.; Chen, J.; Lin, S. H. Tankyrase disrupts metabolic homeostasis and promotes tumorigenesis by inhibiting LKB1-AMPK signalling. *Nat Commun* **2019,** 10, 4363.
7. Chen, B.; Dodge, M. E.; Tang, W.; Lu, J.; Ma, Z.; Fan, C. W.; Wei, S.; Hao, W.; Kilgore, J.; Williams, N. S.; Roth, M. G.; Amatruda, J. F.; Chen, C.; Lum, L. Small molecule-mediated disruption of Wnt-dependent signaling in tissue regeneration and cancer. *Nat.Chem.Biol.* **2009,** 5, 100-107.
8. Waaler, J.; Machon, O.; Tumova, L.; Dinh, H.; Korinek, V.; Wilson, S. R.; Paulsen, J. E.; Pedersen, N. M.; Eide, T. J.; Machonova, O.; Gradl, D.; Voronkov, A.; von Kries, J. P.; Krauss, S. A novel tankyrase inhibitor decreases canonical Wnt signaling in colon carcinoma cells and reduces tumor growth in conditional APC mutant mice. *Cancer Res.* **2012,** 72, 2822-2832.
9. Voronkov, A.; Holsworth, D. D.; Waaler, J.; Wilson, S. R.; Ekblad, B.; Perdreau-Dahl, H.; Dinh, H.; Drewes, G.; Hopf, C.; Morth, J. P.; Krauss, S. Structural basis and SAR for G007-LK, a lead stage 1,2,4-triazole based specific tankyrase 1/2 inhibitor. *J.Med.Chem.* **2013,** 56, 2012-2023.
10. Bregman, H.; Chakka, N.; Guzman-Perez, A.; Gunaydin, H.; Gu, Y.; Huang, X.; Berry, V.; Liu, J.; Teffera, Y.; Huang, L.; Egge, B.; Mullady, E. L.; Schneider, S.; Andrews, P. S.; Mishra, A.; Newcomb, J.; Serafino, R.; Strathdee, C. A.; Turci, S. M.; Wilson, C.; Dimauro, E. F. Discovery of novel, induced-pocket binding oxazolidinones as potent, selective, and orally bioavailable tankyrase inhibitors. *J.Med.Chem.* **2013,** 56, 4320-4342.
11. Anumala, U. R.; Waaler, J.; Nkizinkiko, Y.; Ignatev, A.; Lazarow, K.; Lindemann, P.; Olsen, P. A.; Murthy, S.; Obaji, E.; Majouga, A. G.; Leonov, S.; von Kries, J. P.; Lehtio, L.; Krauss, S.; Nazare, M. Discovery of a novel series of tankyrase inhibitors by a hybridization approach. *J Med Chem* **2017,** 60, 10013-10025.
12. Bregman, H.; Chakka, N.; Guzman-Perez, A.; Gunaydin, H.; Gu, Y.; Huang, X.; Berry, V.; Liu, J.; Teffera, Y.; Huang, L.; Egge, B.; Mullady, E. L.; Schneider, S.; Andrews, P. S.; Mishra, A.; Newcomb, J.; Serafino, R.; Strathdee, C. A.; Turci, S. M.; Wilson, C.; DiMauro, E. F. Discovery of novel, induced-pocket binding oxazolidinones as potent, selective, and orally bioavailable tankyrase inhibitors. *J Med Chem* **2013,** 56, 4320-4342.
13. Haikarainen, T.; Waaler, J.; Ignatev, A.; Nkizinkiko, Y.; Venkannagari, H.; Obaji, E.; Krauss, S.; Lehtio, L. Development and structural analysis of adenosine site binding tankyrase inhibitors. *Bioorg Med Chem Lett* **2016,** 26, 328-333.
14. Nkizinkiko, Y.; Suneel Kumar, B. V.; Jeankumar, V. U.; Haikarainen, T.; Koivunen, J.; Madhuri, C.; Yogeeswari, P.; Venkannagari, H.; Obaji, E.; Pihlajaniemi, T.; Sriram, D.; Lehtio, L. Discovery of potent and selective nonplanar tankyrase inhibiting nicotinamide mimics. *Bioorg Med Chem* **2015,** 23, 4139-4149.
15. McGonigle, S.; Chen, Z.; Wu, J.; Chang, P.; Kolber-Simonds, D.; Ackermann, K.; Twine, N. C.; Shie, J. L.; Miu, J. T.; Huang, K. C.; Moniz, G. A.; Nomoto, K. E7449: A dual inhibitor of PARP1/2 and tankyrase1/2 inhibits growth of DNA repair deficient tumors and antagonizes Wnt signaling. *Oncotarget* **2015,** 6, 41307-41323.
16. Paine, H. A.; Nathubhai, A.; Woon, E. C.; Sunderland, P. T.; Wood, P. J.; Mahon, M. F.; Lloyd, M. D.; Thompson, A. S.; Haikarainen, T.; Narwal, M.; Lehtio, L.; Threadgill, M. D. Exploration of the nicotinamide-binding site of the tankyrases, identifying 3-arylisoquinolin-1-ones as potent and selective inhibitors in vitro. *Bioorg Med Chem* **2015,** 23, 5891-5908.
17. Ferri, M.; Liscio, P.; Carotti, A.; Asciutti, S.; Sardella, R.; Macchiarulo, A.; Camaioni, E. Targeting Wnt-driven cancers: Discovery of novel tankyrase inhibitors. *Eur J Med Chem* **2017,** 142, 506-522.
18. Mizutani, A.; Yashiroda, Y.; Muramatsu, Y.; Yoshida, H.; Chikada, T.; Tsumura, T.; Okue, M.; Shirai, F.; Fukami, T.; Yoshida, M.; Seimiya, H. RK-287107, a potent and specific tankyrase inhibitor, blocks colorectal cancer cell growth in a preclinical model. *Cancer Sci* **2018,** 109, 4003-4014.
19. Buchstaller, H. P.; Anlauf, U.; Dorsch, D.; Kuhn, D.; Lehmann, M.; Leuthner, B.; Musil, D.; Radtki, D.; Ritzert, C.; Rohdich, F.; Schneider, R.; Esdar, C. Discovery and optimization of 2-arylquinazolin-4-ones into a potent and selective tankyrase inhibitor modulating Wnt pathway activity. *J Med Chem* **2019,** 62, 7897-7909.

20. Nathubhai, A.; Haikarainen, T.; Koivunen, J.; Murthy, S.; Koumanov, F.; Lloyd, M. D.; Holman, G. D.; Pihlajaniemi, T.; Tosh, D.; Lehtio, L.; Threadgill, M. D. Highly potent and isoform selective dual site binding tankyrase/Wnt signaling inhibitors that increase cellular glucose uptake and have antiproliferative activity. *J Med Chem* **2017,** 60, 814-820.
21. Sanchez-Vega, F.; Mina, M.; Armenia, J.; Chatila, W. K.; Luna, A.; La, K. C.; Dimitriadoy, S.; Liu, D. L.; Kantheti, H. S.; Saghafinia, S.; Chakravarty, D.; Daian, F.; Gao, Q.; Bailey, M. H.; Liang, W. W.; Foltz, S. M.; Shmulevich, I.; Ding, L.; Heins, Z.; Ochoa, A.; Gross, B.; Gao, J.; Zhang, H.; Kundra, R.; Kandoth, C.; Bahceci, I.; Dervishi, L.; Dogrusoz, U.; Zhou, W.; Shen, H.; Laird, P. W.; Way, G. P.; Greene, C. S.; Liang, H.; Xiao, Y.; Wang, C.; Iavarone, A.; Berger, A. H.; Bivona, T. G.; Lazar, A. J.; Hammer, G. D.; Giordano, T.; Kwong, L. N.; McArthur, G.; Huang, C.; Tward, A. D.; Frederick, M. J.; McCormick, F.; Meyerson, M.; Van Allen, E. M.; Cherniack, A. D.; Ciriello, G.; Sander, C.; Schultz, N. Oncogenic signaling pathways in the cancer genome atlas. *Cell* **2018,** 173, 321-337 e310.
22. Nusse, R.; Clevers, H. Wnt/beta-catenin signaling, disease, and emerging therapeutic modalities. *Cell* **2017,** 169, 985-999.
23. Krishnamurthy, N.; Kurzrock, R. Targeting the Wnt/beta-catenin pathway in cancer: Update on effectors and inhibitors. *Cancer Treat Rev* **2018,** 62, 50-60.
24. Lau, T.; Chan, E.; Callow, M.; Waaler, J.; Boggs, J.; Blake, R. A.; Magnuson, S.; Sambrone, A.; Schutten, M.; Firestein, R.; Machon, O.; Korinek, V.; Choo, E.; Diaz, D.; Merchant, M.; Polakis, P.; Holsworth, D. D.; Krauss, S.; Costa, M. A Novel Tankyrase small-molecule inhibitor suppresses APC mutation-driven colorectal tumor growth. *Cancer Res.* **2013,** 73, 3132-3144.
25. Martins-Neves, S. R.; Paiva-Oliveira, D. I.; Fontes-Ribeiro, C.; Bovee, J.; Cleton-Jansen, A. M.; Gomes, C. M. F. IWR-1, a tankyrase inhibitor, attenuates Wnt/beta-catenin signaling in cancer stem-like cells and inhibits in vivo the growth of a subcutaneous human osteosarcoma xenograft. *Cancer Lett* **2018,** 414, 1-15.
26. Solberg, N. T.; Waaler, J.; Lund, K.; Mygland, L.; Olsen, P. A.; Krauss, S. Tankyrase inhibition enhances the antiproliferative effect of PI3K and EGFR inhibition, mutually affecting beta-catenin and AKT signaling in colorectal cancer. *Mol Cancer Res* **2018,** 16, 543-553.
27. Waaler, J.; Mygland, L.; Tveita, A.; Strand, M. F.; Solberg, N. T.; Olsen, P. A.; Aizenshtadt, A.; Fauskanger, M.; Lund, K.; Brinch, S. A.; Lycke, M.; Dybing, E.; Nygaard, V.; Boe, S. L.; Heintz, K. M.; Hovig, E.; Hammarstrom, C.; Corthay, A.; Krauss, S. Tankyrase inhibition sensitizes melanoma to PD-1 immune checkpoint blockade in syngeneic mouse models. *Commun Biol* **2020,** 3, 196.
28. Fujita, S.; Mukai, T.; Mito, T.; Kodama, S.; Nagasu, A.; Kittaka, M.; Sone, T.; Ueki, Y.; Morita, Y. Pharmacological inhibition of tankyrase induces bone loss in mice by increasing osteoclastogenesis. *Bone* **2018,** 106, 156-166.
29. Norum, J. H.; Skarpen, E.; Brech, A.; Kuiper, R.; Waaler, J.; Krauss, S.; Sorlie, T. The tankyrase inhibitor G007-LK inhibits small intestine LGR5(+) stem cell proliferation without altering tissue morphology. *Biol Res* **2018,** 51, 3.
30. Waaler, J.; Machon, O.; von Kries, J. P.; Wilson, S. R.; Lundenes, E.; Wedlich, D.; Gradl, D.; Paulsen, J. E.; Machonova, O.; Dembinski, J. L.; Dinh, H.; Krauss, S. Novel synthetic antagonists of canonical Wnt signaling inhibit colorectal cancer cell growth. *Cancer Res.* **2011,** 71, 197-205.
31. Krauss, S.; Nazare, M.; Anumala, U.; Lethio, L.; Waaler, J.; Holsworth, D.; Wegert, A.; Leenders, R. Triazole derivates as tankyrase inhibitors (WO/2018/118868). 2018.
32. Sugane, T.; Tobe, T.; Hamaguchi, W.; Shimada, I.; Maeno, K.; Miyata, J.; Suzuki, T.; Kimizuka, T.; Sakamoto, S.; Tsukamoto, S. Atropisomeric 4-phenyl-4H-1,2,4-triazoles as selective glycine transporter 1 inhibitors. *J Med Chem* **2013,** 56, 5744-5756.
33. Laplante, S. R.; L, D. F.; Fandrick, K. R.; Fandrick, D. R.; Hucke, O.; Kemper, R.; Miller, S. P.; Edwards, P. J. Assessing atropisomer axial chirality in drug discovery and development. *J Med Chem* **2011,** 54, 7005-7022.
34. Narwal, M.; Fallarero, A.; Vuorela, P.; Lehtio, L. Homogeneous screening assay for human tankyrase. *J Biomol Screen* **2012,** 17, 593-604.
35. Venkannagari, H.; Fallarero, A.; Feijs, K. L.; Luscher, B.; Lehtio, L. Activity-based assay for human mono-ADP-ribosyltransferases ARTD7/PARP15 and ARTD10/PARP10 aimed at screening and profiling inhibitors. *Eur J Pharm Sci* **2013,** 49, 148-156.
36. Venkannagari, H.; Verheugd, P.; Koivunen, J.; Haikarainen, T.; Obaji, E.; Ashok, Y.; Narwal, M.; Pihlajaniemi, T.; Luscher, B.; Lehtio, L. Small-molecule chemical probe rescues cells from mono-ADP-Ribosyltransferase ARTD10/PARP10-induced apoptosis and sensitizes cancer cells to DNA damage. *Cell Chem Biol* **2016,** 23, 1251-1260.
37. Murthy, S.; Desantis, J.; Verheugd, P.; Maksimainen, M. M.; Venkannagari, H.; Massari, S.; Ashok, Y.; Obaji, E.; Nkizinkinko, Y.; Luscher, B.; Tabarrini, O.; Lehtio, L. 4-(Phenoxy) and 4-(benzyloxy)benzamides as potent and selective inhibitors of mono-ADP-ribosyltransferase PARP10/ARTD10. *Eur J Med Chem* **2018,** 156, 93-102.
38. Kabsch, W. Xds. *Acta Crystallogr D Biol Crystallogr* **2010,** 66, 125-132.
39. McCoy, A. J.; Grosse-Kunstleve, R. W.; Adams, P. D.; Winn, M. D.; Storoni, L. C.; Read, R. J. Phaser crystallographic software. *J Appl Crystallogr* **2007,** 40, 658-674.
40. Emsley, P.; Cowtan, K. Coot: model-building tools for molecular graphics. *Acta Crystallogr D Biol Crystallogr* **2004,** 60, 2126-2132.
41. Murshudov, G. N.; Skubak, P.; Lebedev, A. A.; Pannu, N. S.; Steiner, R. A.; Nicholls, R. A.; Winn, M. D.; Long, F.; Vagin, A. A. REFMAC5 for the refinement of macromolecular crystal structures. *Acta Crystallogr D Biol Crystallogr* **2011,** 67, 355-367.

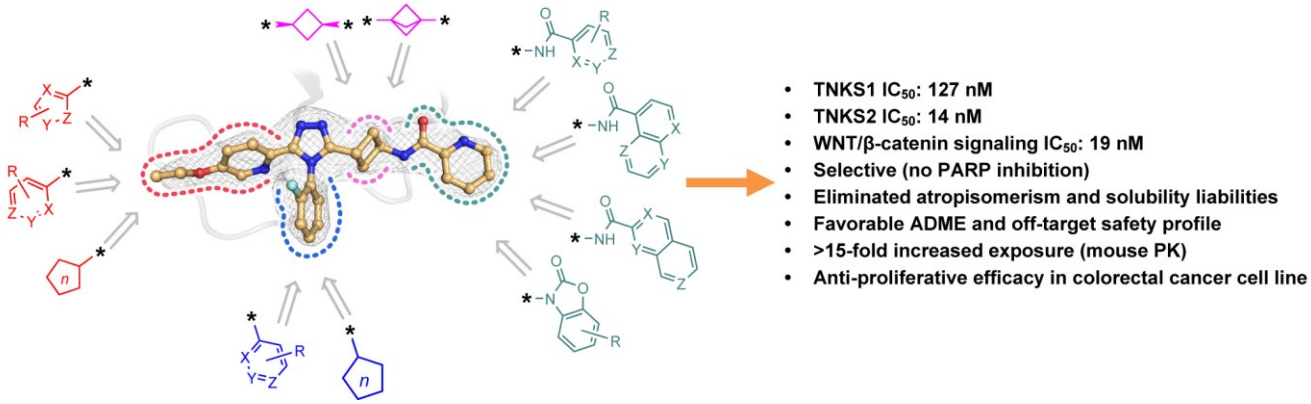

Synopsis TOC Graphic